

Rotorcraft Lateral-Directional Oscillations: The Anatomy of a Nuisance Mode

Dheeraj Agarwal

Assistant Professor,

Birla Institute of Technology and Sciences, Pilani, Hyderabad Campus

Hyderabad, India

Linghai Lu (Corresponding author, Email: L.LU@cranfield.ac.uk)

Senior Lecturer,

Cranfield University,

Cranfield, United Kingdom

Gareth D. Padfield

Emeritus Professor,

University of Liverpool,

Liverpool, United Kingdom

Mark D. White

Professor,

University of Liverpool,

Liverpool, United Kingdom

Neil Cameron

Research Fellow,

University of Liverpool,

Liverpool, United Kingdom

Abstract

High fidelity rotorcraft flight simulation relies on the availability of a quality flight model that further demands a good level of understanding of the complexities arising from aerodynamic couplings and interference effects. One such example is the difficulty in prediction of the characteristics of the rotorcraft lateral-directional oscillation (LDO) mode in simulation. Achieving an acceptable level of the damping of this mode is a design challenge requiring simulation models with sufficient fidelity that reveal sources of destabilizing effects. This paper is focused on using System Identification to highlight such fidelity issues using Liverpool's FLIGHTLAB Bell 412 simulation model and in-flight LDO measurements from the bare airframe National Research Council's (Canada) Advanced Systems Research Aircraft. The simulation model was renovated to improve the fidelity of the model. The results show a close match between the identified models and flight test for the LDO mode frequency and damping. Comparison of identified stability and control derivatives with those predicted by the simulation model highlight areas of good and poor fidelity.

Nomenclature

I_{xx}, I_{yy}, I_{zz}	moment of inertia of the helicopter in roll, pitch and yaw [slug-ft ²]
I_{xz}	product of inertia of the helicopter about the roll and yaw axes [slug-ft ²]
K_β	flap hinge spring stiffness [ft-lbf/rad]
L_{lat}, N_{ped} etc.	control derivatives normalized by moments of inertia [rad/(s ² -inch)]
L_v, N_r etc.	moment derivatives normalized by moments of inertia [rad/(s-ft), 1/s etc.]
M_β, I_β	first and second flap moments of inertia [slug-ft, slug-ft ²]
M_ζ, I_ζ	first and second lag moments of inertia [slug-ft, slug-ft ²]
p, r	angular velocity components of helicopter about fuselage x, z axes [deg/s, rad/s]
Q_{dyn}	dynamic pressure at tail relative to free stream [%]
U_e	trim velocity along the helicopter x axis [ft/s]
v	velocity along helicopter y axis [ft/s]
\dot{v}	rates of change of v velocity [ft/s ²]
V_{NE}	never exceed speed
V_Y	best rate of climb speed
Y_v, Y_r etc.	Y force derivatives normalized by aircraft mass [1/s, ft/(s·rad) etc.]
$\delta_{lat}, \delta_{ped}$	pilot lateral cyclic and pedal inputs [inch]
ζ, ζ_d	relative damping and Dutch roll damping ratio
τ_{lat}, τ_{ped}	effective time delay in lateral and pedal channel [s]
ω_n, ω_d	modal natural frequency and damped natural frequency [rad/s]

Acronyms

ADS	Aeronautical Design Standard
AGARD	Advisory Group for Aeronautical Research and Development
ASRA	Advanced Systems Research Aircraft
BIUG	Background Information and User Guide (for ADS-33)
CAT	Category
CS	Certification Specification
CS-FSTD(H)	Certification Specifications - Flight Simulation Training Devices (Helicopter)
DoF	Degree-of-Freedom
DPL	Dynamic Pressure Loss
FS	Flight Simulation
FT	Flight Test
GARTEUR	Group for Aeronautical Research and Technology in Europe
HQs	Handling Qualities
IFR	Instrument Flight Rules
IMC	Instrument Meteorological Conditions
LDO	Lateral Directional Oscillation
MTE	Mission Task Element
NRC	National Research Council
SID	System Identification
SCAS	Stability and Control Augmentation System
TA&T	Target Acquisition and Tracking
VMC	Visual Meteorological Conditions

Introduction

Predicting the damping and frequency of the rotorcraft lateral-directional oscillation (LDO) through modeling and simulation has proved notoriously difficult. Padfield (Ref. 1, 2) describes analyses carried out on three helicopters by the Advisory Group for Aeronautical Research and Development (AGARD) System IDentification (SID) working group WG-18 in the early 1990s, that showed damping predictions were typically double those measured in flight using SID methods. Fig. 1 shows these results for the bare airframe and includes the handling qualities (HQs) level boundaries from the military standard at the time, Aeronautical Design Standard ADS-33C (Ref. 3). As noted in (Ref. 4), the HQ level boundaries in ADS-33 are derived from earlier fixed-wing criteria (Ref. 5) as discussed below. The simulation models used in (Ref. 1) were typical of the time, featuring disc, or first-generation blade-element, main rotors and Bailey disc tail rotors (Ref. 6), and very simple interactional aerodynamics. For completeness, the values of the LDO stability characteristics for the National Research Council of Canada (NRC) Bell 412 Advanced Systems Research Aircraft (ASRA) and nonlinear FLIGHTLAB simulation (Ref. 7) model (F-B412) used (Ref. 8) in the present research are included in Fig. 1. The LDO frequency (vertical axis) and damping (horizontal axis) are shown in terms of the modal natural frequency (ω_n) and relative damping (ζ).

The boundary lines in Fig. 1 deserve a description. The qualification/certification requirements for the damping of LDOs are set out in the military standard, ADS-33 (Ref. 3), the European civil standard, CS-29, and the American civil standard, AC-29, for flight under instrument flight rules (IFR) (Ref. 9, 10). The ADS-33 boundaries are largely based on the fixed-wing military aircraft standards, MIL-F-8785C (Ref. 11), for the Dutch roll mode. One significant difference is the Level 1-2 boundary for “*Target*

Acquisition and Tracking” (TA&T, previously “*slalom, ground attack and air combat*”) tasks. This is an extension of the 0.35 relative damping (ζ) boundary line for yaw oscillations in low-speed tasks flown with divided attention. (Ref. 4) states that there are “*no quantitative data to support this limit in forward flight. The intent is the same, however, since excessive lateral-directional oscillations in a high workload environment, will result in degraded handling qualities at any speed*”. The 0.19 relative damping (ζ), and $\zeta\omega_n = 0.35$, lines, correspond to the Level 1-2 boundary for fixed-wing aircraft in Category (CAT) A flight phases (e.g. “*rapid maneuvering and precision tracking*”). ADS-33 adopts this as the Level 1-2 boundary for “*all other MTEs*”, and Level 2-3 boundary for TA&T tasks, although (Ref. 4) states that, “*the representation of this boundary as the Level 2 limit for slalom, ground-attack and air combat is less supportable, and is based on convenience of format*”. The Level 2-3 boundary ($\zeta > 0.02$, $\zeta\omega_n > 0.05$) and (zero ζ) Level 3-4 boundary accord with the fixed-wing military aircraft standard.

CS-29 states that the aircraft only needs to be stable for flight in Visual Meteorological Conditions (VMC); effectively the vertical, zero damping, line in Fig. 1. These lines have been derived from the CS-29. Note that these are not Level 1-2 boundaries as such, as the culture of civil standards does not admit this categorization. The standards for acceptable HQs in IFR flight are drawn from the early MIL-STD-8501 (Ref. 12) criteria where the allowable number of cycles to half amplitude is prescribed as a function of the LDO period. For oscillations with a period of fewer than 5 seconds, the time to half amplitude must be less than one cycle. So, above a frequency of 1.26 rad/sec, the boundary follows the $\zeta \approx 0.11$ line as shown in Fig. 1. In discussing results from flight trials exploring fixed-wing aircraft LDO characteristics during flight in turbulence, Franklin (Ref. 13) concludes that “*Increasing the Dutch roll damping*

ratio improves flying qualities for the lowest level of directional stability tested ($\omega_d = 1.3$ rad/sec). No improvement with increased ζ_d (from 0.1 to 0.4) occurs for the configuration having the highest directional stability tested ($\omega_d = 3.0$ rad/sec)". It should be emphasized that, for both civil and military standards, the LDO is the only 'mode' for which there are requirements on stability for forward flight operations; ADS-33 includes stability requirements on pitch and roll oscillations for low-speed tasks.

There are some outstanding questions stemming from this historical perspective. First, for the most demanding military helicopter tasks, is the minimum relative damping of 0.35 really required? Second, is a minimum relative damping of 0.19 sufficient for Level 1 HQs in general MTEs? Third, how close to zero damping is acceptable for Level 2 performance? Is a ζ of 0.2 sufficient? Considering Franklin's conclusion, the insensitivity of pilot opinion on the impact of relative damping at higher LDO frequencies warrants further investigation, although it does seem to concur with the civil standards. Perhaps more significant a question is whether the 0.11 line is sufficient as a minimum standard for civil operations in IFR flight? It is not the intention of this paper to address all these questions, but rather to present results from our fidelity renovation process in advance of ongoing HQ investigations and the development of a piloted-simulation trial methodology.

Fig. 1 defines minimum acceptable levels considered appropriate for military and civil operations, respectively. The poor levels of natural rotorcraft LDO damping normally mean that stability augmentation is required to achieve the minimum standards for military aircraft operating with divided (pilot) attention or in degraded visual conditions, and civil aircraft operating in instrument meteorological conditions (IMC). The level of augmentation, constrained by the authority of the series actuators

and the gains in the automatic control system feedback loops, is then determined by the design damping margin. In a worst-case scenario, poor (too high) predictions of damping in the design phase could lead to inappropriate (too low) levels of feedback gain which may then need to be corrected during flight test (FT) development, impacting the design of the actuation system.

Achieving an acceptable level of natural LDO damping is a design challenge requiring simulation models with sufficient fidelity that reveal sources of destabilizing effects. Understanding the sources of modeling deficiencies is aided by a systematic approach to the comparison of flight and simulation responses and the analysis of any differences and their physical sources. SID provides this for the comparative aspects, and recent developments have enabled the differences to be transformed into model updates or renovations that reflect the missing physics. The SID approach has been extensively used in the research field of fixed-wing aircraft (Ref. 14, 15) and rotorcraft (Ref. 8, 16-21) for performance and HQs evaluation, control law development, aircraft dynamic loads analysis, and the creation of a realistic piloted simulation environment.

On a closely related theme, helicopter flight (simulation) training devices are qualified using guidance contained within e.g., Certification Specifications - Flight Simulation Training Devices (Helicopter), (CS-FSTD(H)) (Ref. 22) which details the acceptable match between flight and simulation time histories. A model is considered 'acceptable' if the differences between the histories are within certain tolerances e.g. match of angular attitudes and velocities within $\pm 10\%$ following a step control input. GARTEUR HC-AG12 (Ref. 23) showed that, in most areas, 80% "*fidelity*" should be achievable with physical modelling but that the remaining 20% requires artificial tuning; this last 20% is critical for simulator qualification.

In this paper, SID methods are used to gain insight into the contributing stability derivatives and related design features of the aircraft. The renovation method based on the work of Lu et. al. (Ref. 21) has been applied to improve the predictive fidelity of Liverpool's nonlinear FLIGHTLAB flight simulation model of the NRC's ASRA, designated as F-B412. This paper starts with a discussion of the characteristics, the anatomy, of the rotorcraft LDO mode, followed by a detailed investigation of the LDO characteristics of the F-B412. Afterwards, the SID technique in the frequency domain is used to obtain 3 Degree-of-Freedom (DoF) and 6DoF linear models, and subsequently use these to improve the fidelity of the F-B412. An effort then is made to link the modeling deficiencies with the physical sources. The end of the paper draws the conclusions of the research.

The Anatomy of the Lateral-Directional Oscillatory Mode

The Dutch roll, or more generally LDO, mode has historically been described as a 'nuisance' mode, in the sense that the coupled yaw-roll-sway dynamics contribute nothing useful to the aircraft performance and handling but, rather, any excitation needs to be compensated by pilot control action. The mode is thus a contributor to HQs deficiencies. The extent of those deficiencies, and the required pilot control compensation, depends critically on the damping and frequency, as discussed, but also on the amplitude ratio of roll to yaw/sideslip in the mode and the associated phase between these motions. For example, a yaw-dominant LDO, as found on a wide variety of fixed-wing aircraft, usually requires complementary control compensation, i.e. a right yaw is accompanied by a right roll, hence left pedal and left stick compensation. For rotorcraft, the roll/yaw ratio in the LDO is often unity, or even greater, and the phase between the motions can require more complex pilot compensation. Fig. 2, from Padfield

(Ref. 1), shows a comparison between roll and yaw rates during the Dutch roll mode for the Puma helicopter (SA330) in descending, level and climbing flight. In descent, the roll/yaw (p/r) ratio is about 0.8, increasing to 1.2 in level flight and about 2 in a climb. The Super Puma Dutch roll response presented in Casolaro et al. (Ref. 24) shows an even larger p/r ratio of about 4 for a 125 kts level flight case (Fig. 3).

The reason for the large p/r ratio in the LDO for rotorcraft is not straightforward, but several factors are involved. First, a typical helicopter's roll moment of inertia (I_{xx}) is much smaller than the yaw moment of inertia (I_{zz}); Padfield (Ref. 1) reports the Puma's I_{zz}/I_{xx} to be approximately 3. Second, the natural yaw damping and stiffness from the fin and tail rotor can both be weak. The tail rotor loses damping effectiveness as forward speed increases and the use of thick aerofoil sections for the fin, to accommodate the driveshaft and gearbox, can reduce the surface's lift effectiveness at small angles of sideslip. Both these aspects are discussed in Padfield (Ref. 1). Third, a helicopter is trimmed in forward flight with a negative main rotor disc incidence. Fuselage roll then results in the dihedral (L_v) from the rotor acting to increase the roll, even though L_v itself is negative. The opposite occurs for rotorcraft in descending flight and for fixed-wing aircraft that normally fly in trim with the wings at positive incidence relative to the fuselage. Fourth, the principal axes of inertia for a helicopter are rarely aligned with the fuselage waterline (x -axis), so it is usual for the product of inertia of the helicopter about the roll and yaw axes, I_{xz} , to be non-zero with consequential impact on coupling derivatives like N_p and L_r . Fifth, the vertical fin and tail rotor are typically in a velocity depression due to the blockage effects from the upper fuselage and rotor hub.

The nuisance factor of the LDO mode for a helicopter is therefore much greater than its fixed-wing counterpart. For example, from Fig. 2, in the climb, the yaw is about

90 deg ahead of the roll. When the aircraft has a maximum yaw rate (at about 9 sec), it is at its maximum negative roll angle; corrective compensation by the pilot requires cross controls, left pedal and right cyclic. A similar situation was described for the Super Puma in Casolaro et al. (Ref. 24), where the aircraft was unstable (Fig. 3). In VMC flight the pilots *“concluded that the simulator was handling like the real helicopter. However, when conducting the same test in IMC, the pilots complained that the model was too unstable and too difficult to manage.”* In Casolaro et al. (Ref. 24) the authors conjecture that the *“distorted accelerations provided by the motion system and the delay introduced by the visual system might be the explanation.”* The pilot reported that he was *“unable to stop the Dutch roll oscillations and asked for a higher damping to reproduce the flight behaviour.”* The flight model had been ‘tuned’ to match the flight data and this example highlights a situation where pilot opinion can lead to adjustments that result in mismatches in the flight model response. So, not only is the LDO mode difficult to suppress but it can also lead to contradictions between quantitative and qualitative assessments, or between the predicted and perceptual fidelity.

Case Study – Predicting the LDO with the F-B412

Test Aircraft and Flight Test Data

The reference aircraft is the National Research Council of Canada’s Bell 412 ASRA (Ref. 25) illustrated in Fig. 4. The ASRA is specially configured with onboard research equipment for the development and testing of advanced flight control systems and modern cockpit technologies. Specialized research equipments installed in the aircraft include a fly-by-wire control system (mechanical back-up with safety pilot), force feel system, and data acquisition system with graphical display capability. In 2018, the

ASRA completed extensive upgrades that included new engines with improved torque dynamics and a glass cockpit with ‘modernized’ avionics.

Flight test campaigns were performed on the ASRA in 2004–6 and 2009–11 to support control law design (Ref. 26) and simulation fidelity research (Ref. 21, 27–29) respectively at Liverpool. Open-loop responses to control steps, pulses, 2311s, and sweeps have been measured throughout the flight envelope with Stability and Control Augmentation System (SCAS) on and off. Closed-loop MTEs have also been flown. This paper focuses on bare-airframe (i.e. SCAS off) flight dynamics at 90kts, mainly from the 2004–6 dataset, consisting of Doublet, 2311 and frequency sweep control inputs.

Model Development

The baseline model used in this work is the F-B412 (Ref. 8) created using the multi-body-dynamic modeling tools of the FLIGHTLAB simulation environment (Ref. 7). It features a blade-element main rotor with non-linear aerodynamics and a Bailey disc tail rotor (Ref. 6). The hingeless rotor is represented by rigid blades with hinge-offset-spring analogues for flap and lag dynamics. The fuselage and empennage aerodynamic forces and moments are derived from non-linear look-up tables. Table 1 lists some of the key F-B412 engineering parameters.

Predicting the LDO Mode Characteristics

Fig. 5 shows the predicted F-B412 LDO mode characteristics as a function of flight velocity, stemming from the lateral phugoid at 40 knots (lower right point). The impact of flight path angle (rate of descent +1000, 0, -1000 ft/min) on the LDO roll/yaw ratio and stability are shown in Fig. 6 and **Fig. 7**. These variations are related to the variation of the dihedral and weathercock stability as shown in Table 2. The dihedral (L_v)

increases in magnitude and the weathercock (N_v) decreases across these flight conditions, both contributing to the 50% reduction in damping of the LDO.

An initial comparison of the flight dynamics of the F-B412 with FT is given in Fig. 8, showing the lateral-directional responses of the aircraft to pedal and lateral cyclic 2311 multi-step inputs at the 90kts flight condition. The shaded areas on the responses denote the range of acceptable fidelity tolerance according to (Ref. 22). Roll from lateral cyclic shows very good fidelity, but the fidelity of roll from pedal and yaw and sideslip from pedal is generally poor. SID can now be used to explore whether fidelity deficiencies are reflected in differences between specific stability and control derivatives from flight and simulation.

Estimating LDO Dynamics Using SID

Lateral-Directional Model Approximation

If coupling effects are weak, the 6DoF rotorcraft linear model can be divided into two 3DoF linear models: the yaw/roll/sway and surge/pitch/heave. To establish the fidelity of the 3DoF lateral-directional model, SID using the Comprehensive Identification from Frequency Responses (CIFER) software (Ref. 18) in the frequency domain is applied to this model structure, using the Bell 412 FT data at a flight condition of 90 knots straight and level flight, 3000 ft above ground level. The SID is performed using the piloted frequency-sweep FT data and the results for the lateral-directional stability and control derivatives (3DoF model) are shown in Table 3, including the parameter standard deviations (std), and a comparison with those of linear F-B412 (LF-B412) values, using a standard backward-forward differencing method. The time responses from FT are compared with those obtained from the SID (3DoF and 6DoF) and F-B412 models in Fig. 9 for multi-step inputs in lateral cyclic and pedal. As

expected, the SID model shows an improved match with FT, compared with the F-B412. Notable differences in the stability derivatives in Table 3 are N_v showing a large (70%) reduction relative to the LF-B412, Y_v showing a 20% increase, and N_r a 20% reduction. Roll from pedal, L_{ped} , shows a 20% reduction and yaw from cyclic, N_{lat} , a 30% increase. These differences reflect the time response mismatches of course and will also impact the prediction of the LDO frequency and damping. The good match for the 3DoF SID model, compared with the 6DoF SID model and FT, shown in Fig. 9 is encouraging for LDO prediction using the lateral-directional dynamic approximation.

LDO Eigenvalues

The LDO mode eigenvalues derived from the (stability) derivatives and the 2nd order approximations from Padfield (Ref. 1), are shown in Table 4. Here, the eigenvalues for the 3DoF model structure are compared with those for the 6DoF model structure. As expected, the real aircraft is less stable than predicted by the F-B412, with a much lower mode frequency. Significantly, the LDO eigenvalues from FT obtained using 3DoFs are within 2% of the 6DoF SID models (Ref. 18). This suggests that the couplings from surge, heave and pitch have little impact on the key LDO dynamic characteristics. Both the LDO frequency, dominated by the contribution from N_v , and damping are consistently over-predicted by the F-B412. The comparisons are brought into stark contrast in Fig. 10, showing the LDO characteristics on the HQs chart, described earlier in the paper (Fig. 1).

LDO Fidelity Improvement Using Renovation

In the renovation process, summarized in Fig. 11, deficiencies in the fidelity of F-B412, or the mismatch between FT and flight simulation (FS), are corrected with incremental forces and moments as ‘delta’ derivatives. These deltas are derived from

comparisons of the parameters in the SID and LF-B412 derivative model. More details of the renovation methodology are given in Lu et al. (Ref. 21). In this application, we are concerned with renovating the F-B412 for the prediction of the LDO characteristics. Pitch and heave dynamics are therefore not renovated, and the 3DoF model structure is adopted.

The renovation method selects the derivatives which are effective in improving the match between the FT and F-B412 responses in terms of the impact on defined cost functions. The required changes in these derivatives (Δs) are established by comparing the values in Table 3. The renovation algorithm minimizes the defined cost functions (Ref. 21) to derive the best fit using the selected derivatives. The results of the renovation of the F-B412 (RF-B412) are summarized in Table 5. Fig. 12 shows the responses of the RF-B412 to the multi-step control inputs compared with FT, the baseline F-B412, and the 3DoF SID model. The comparisons confirm the good quality match, as assessed by the CS-FSTD(H) tolerances, of the linear SID 3DoF model has been preserved in the RF-B412. This model is not only nonlinear of course, but includes the ‘higher-order’ dynamics from, e.g. the rotor flapping/lagging and rotor wake. The FSTD(H) requires on-axis responses to be within the boundary and off-axis responses to be in the correct direction, however the boundaries added to the off-axis response aims to show that the method is not only capable of satisfying the CT&M requirements but the improvement is such that it is in line with the on-axis requirements.

The LDO mode eigenvalues from renovation using an increasing number of stability derivatives are shown in Table 6. As before, the F-B412 is more stable than the ‘real’ aircraft, with a higher mode frequency. Also, included in Table 6 are the eigenvalues predicted using the 2nd-order approximations from Padfield (Ref. 1). The renovated 3DoF lateral-directional model features a modal damping and frequency

mismatch of only 2% relative to the 6DoF results. The points for the RF-B412 are shown on the eigenvalue chart in Fig. 13, with the $\pm 10\%$ box centered on the FT indicating the limits for flight simulator qualification tolerance bounds (Ref. 22, 30).

Exploration of Potential Physical Contributions to the Prediction of N_v

The close match shown in Fig. 13 between the renovated simulation and flight for the LDO frequency and damping has been achieved through the renovation of just three stability derivatives; the static stability derivatives N_v and L_v and the yaw damping N_r , bringing frequency and damping close to FT. This might be sufficient to ensure a satisfactory fit for both military and civil HQs standards. However, although systematic and rational, the SID approach does not shed light on the physical source of the mismatch. The large change required to N_v is undoubtedly the most concerning from a fidelity standpoint. Fig. 14 shows a breakdown of the contributions to N_v from the various components in the F-B412. The tail fin and tail rotor provide positive contributions to stability, so it is perhaps to these components that attention could be drawn for some understanding of the fidelity enhancement.

As noted above, the renovation method does not identify the source of the modeling errors but the absence of interference between the main rotor wake, fuselage and rotor hub and the tail and tail rotor is a candidate. Fig. 15 shows a comparison of the response of the F-B412 with FT with and without rotor interference on the tailfin and tail rotor. The contracting 3-state rotor inflow is carried downstream with downwash and side-wash velocities eventually impacting the tail. The process is time-dependent and inherently nonlinear but FLIGHTLAB does enable a linearization of the effects to provide a first-order prediction of the stability derivatives. The dihedral effect and yaw damping are hardly affected by interference but the weathercock derivative, N_v ,

decreases by about 25% (0.018 compared to 0.024 (Table 3)), a step in the right direction.

An altogether more powerful interference effect leads to a dynamic pressure loss (DPL) at the tail caused by the flow blockage from the upper fuselage and hub. The FLIGHTLAB implementation requires a 3D data table, with pressure loss as a function of the local incidence and sideslip angles. Such a table could be created from, for example, wind tunnel data or more refined wake calculations, including from a computational fluid dynamics analysis. In the absence of such data for the B412, Fig. 16 shows how the weathercock effect and the location of the LDO eigenvalue are modified by the DPL at the tail. To match the FT estimate of N_v requires a 30% reduction in dynamic pressure at the tail, also resulting in a closer fit to the LDO eigenvalues. Fig. 17 shows a comparison of the response of the F-B412 to the pedal multi-step with FT, with and without the 30% DPL. The close match with FT for p , r and v is in contrast with the results in Fig. 15, showing the impact of the rotor wake on the tail.

These effects of aerodynamic interference on the tail should not be totally unexpected. References (Refs. 31, 32) report results from wind tunnel testing on the BK117 and SA365N, showing DPL at the tail surfaces caused by interference from the flow over the rotor hub and upper fuselage. For both aircraft, centers of depression as low as 50% of free-stream dynamic pressure are shown with strong lateral and vertical gradients. For both aircraft, unsteady interference resulted in ‘tail-shake’ vibrations that were cured through improved upper fuselage and tail design. In the case of the BK117, the 11% LDO ζ requirement for IFR flight was achieved through a re-design of the tail surfaces; to quote from (Ref. 31), “*the main solution was achieved by a change of the endplates configuration, consisting of an increase of the fin area, and of optimization*

of the fin shape for negative flow angles of attack”.

One final investigation of interference effects involves representing the delayed impact of the rotor wake on the tail (hysteretic damping), in much the same way as incidence rate effect on fixed and rotary-wing aircraft can be approximated by the addition of an $M_{\dot{w}}$ derivative, augmenting the pitch damping M_q . In the case of lateral-directional motion, the equivalent moment due to delayed side-wash effects, comes from the $N_{\dot{v}}$ derivative. Fig. 18 shows the impact of this effect on the yaw response of the F-B412 from a pedal multi-step. An arbitrary variation of 10% of the primary N_v effect is shown, the main result being to increase ($+N_{\dot{v}}$) or reduce ($-N_{\dot{v}}$) the damping (effective N_r) of the response. The impact on the static stability derivatives N_v and L_v is negligible.

Conclusions

This paper has addressed the topic of predicting the characteristics of the Lateral-Directional Oscillation (LDO, aka Dutch roll) mode for rotorcraft. The LDO handling qualities charts and level boundaries for military and civil operations form a template for the simulation fidelity analysis. The paper has provided a brief history of these standards, which have generally been derived from the fixed-wing ‘story’. The baseline simulation model used was the F-B412, a multi-body-dynamic nonlinear model of the Bell 412 aircraft, created using the FLIGHTLAB simulation software environment. Test data from the Canadian NRC’s ASRA 412 research aircraft were used to support the simulation fidelity assessment, specifically from a 90kts straight and level flight condition. System Identification, using the frequency domain CIPHER algorithms, was used to estimate the stability and control derivatives and create linear models to explore fidelity issues. A model-updating or ‘renovation’ process has been presented whereby

fidelity improvements to the F-B412 are made using derivative ‘deltas’. The main conclusions of the research addressed in this paper are:

1) Based on a comparison of (flight and simulation) results from 6 Degree of Freedom (DoF) and 3DoF model structures, the main elements of the LDO can be identified in the 3DoF roll-sway-yaw dynamics.

2) A baseline simulation model of the Bell-412 helicopter, the F-B412, captures the essential features of the LDO but significant deficiencies in the prediction of frequency have been identified.

3) The renovation analysis predicted that close agreement could be achieved with flight through augmenting the F-B412 with ‘deltas’ in the derivatives N_v , L_v , and N_r . The renovation achieves a modal damping and frequency match within 2% of the flight test.

4) Physical sources of modeling deficiencies have been investigated, with the interaction of the wake from the main rotor hub and upper fuselage being the strongest candidate. Including a general model of dynamic pressure reduction at the tail achieves a close match with flight test. However, the conclusion from this analysis is regarded as tentative, in need of further investigation.

Acknowledgements

Contributions from staff at the National Research Council of Canada are acknowledged, particularly the ASRA facility manager, Bill Gubbels. The research reported in this paper is funded by the UK’s Engineering and Physical Sciences Research Council (EP/P031277/1 and EP/P030009/1). The reported research is also contributing to the NATO STO AVT-296 activity, ‘*Rotorcraft flight simulation model fidelity improvement and assessment*’.

References

- ¹Padfield, G.D., “*Helicopter Flight Dynamics: Including a Treatment of Tiltrotor Aircraft*,” Third Ed. John Wiley & Sons, 2018, Chapter 4, 5.
- ²Padfield, G.D., and DuVal, R.W., “Application Areas for Rotorcraft System Identification: Simulation Model Validation,” AGARD, LS-178, November 1991.
- ³Anon., “ADS-33E-PRF, Handling Qualities Requirements for Military Rotorcraft,” U.S. Army AMCOM, Redstone, AL. (A version 1987, B version 1988, C version 1989, D version, 1994, D-PRF version 1996, E-PRF version 2000), March 2000.
- ⁴Key, D.I., Blanken, C.L., Hoh, R.H., Mitchell, D.G., and Aponso, B.L., “Background Information and User’s guide (BIUG) for Handling Qualities Requirements for Military Rotorcraft,” U.S. Army Research, Development, and Engineering Command, Special Report RDMR-AD-16-01, December 2015.
- ⁵Anon., “Military Specification - Flying Qualities of Piloted Airplanes,” MIL-F-8785C, November 1980.
- ⁶Bailey Jr, F., “A simplified theoretical method of determining the characteristics of a lifting rotor in forward flight,” NACA, 716, 1941.
- ⁷DuVal, R.W., and He, C., “Validation of the FLIGHTLAB Virtual Engineering Toolset,” *The Aeronautical Journal*, Vol. 122, (1250), 2018, pp. 519-555, DOI: 10.1017/aer.2018.12.
- ⁸Cameron, N., White, M.D., Padfield, G.D., Lu, L., Agarwal, D., and Gubbels, A.W., “Rotorcraft Modelling Renovation for Improved Fidelity,” 75th Annual Forum of America Helicopter Society, Philadelphia, PA, May 13-16, 2019.
- ⁹Anon., “Certification Specifications and Acceptable Means of Compliance for Large Rotorcraft CS-29,” EASA, Amendment 7, 15 July 2019.

¹⁰Anon., “AC-29-2C, Certification of Transport Category Rotorcraft,” Federal Aviation Administration, Advisory Circular, 2014.

¹¹Moorhouse, D.J., and Woodcock, R.J., “Background Information and User Guide for MIL-F-8785C, Military Specification-Flying Qualities of Piloted Airplanes,” U.S. Air Force Wright Aeronautical Labs Wright-Patterson AFB OH, 1982.

¹²Anon., “Military Specification - General Requirements for Helicopter Flying and Ground Handling Qualities,” MIL-H-8501A, 1961, superseding MIL-H-8501.

¹³Franklin, J.A., “Turbulence and Lateral-Directional Flying Qualities,” NASA CR1718, April 1971.

¹⁴Drobik, J.S., and Brian, G.J., “Application of System Identification Techniques to the F-111C and PC 9/A Aircraft,” *Journal of Aircraft*, Vol. 41, (4), 2004, pp. 744-751, DOI: 10.2514/1.4993.

¹⁵Morelli, E.A., and Klein, V., “Application of System Identification to Aircraft at NASA Langley Research Center,” *Journal of Aircraft*, Vol. 42, (1), 2005, pp. 12-25, DOI: 10.2514/1.3648.

¹⁶Padfield, G.D., Thorne, R., Murray-Smith, D., Black, C., and Caldwell, A.E., “UK Research into System Identification for Helicopter Flight Mechanics,” *Vertica*, Vol. 11, (4), 1987, pp. 665-684,

¹⁷Hamel, P.G., and Kaletka, J., “Advances in Rotorcraft System Identification,” *Progress in Aerospace Sciences*, Vol. 33, (3-4), 1997, pp. 259-284, DOI: 10.1016/S0376-0421(96)00005-X.

¹⁸Tischler, M.B., and Remple, R.K., “*Aircraft and Rotorcraft System Identification*,” 2nd Ed. AIAA, 2012, Chapters 9, 10, 12 13.

¹⁹Wei, W., Cohen, K., and Tischler, M.B., “System Identification and Controller Optimization of a Quadrotor UAV,” 71st Annual Forum of the American Helicopter Society, Virginia Beach, VA, May 5-7, 2015.

²⁰Scher-Weiss, S., Greiser, S., Wartmann, J., Gubbels, A.W., Ricciardi, J., and Hui, K., “Bell 412 System Identification: Comparing Methods and Tools,” 75th Annual Forum of the American Helicopter Society, Philadelphia, PA, May 12-16, 2019.

²¹Lu, L., Padfield, G.D., White, M.D., and Perfect, P., “Fidelity Enhancement of a Rotorcraft Simulation Model Through System Identification,” *The Aeronautical Journal*, Vol. 115, (1170), 2011, pp. 453-470, DOI: 10.1017/S0001924000006102.

²²Anon., “CS-FSTD(H), Helicopter Flight Simulation Training Devices.” EASA, Initial issue, 26 June 2012.

²³Pavel, M., White, M.D., Padfield, G.D., Roth, G., Hamers, M., and Taghizad, A., “Validation of Mathematical Models for Helicopter Flight Simulators Past, Present and Future Challenges,” *The Aeronautical Journal*, Vol. 117, (1190), 2013, pp. 343-388, DOI: 10.1017/S0001924000008058.

²⁴Casolaro, D., Dequin, A., and Gaulene, P., “Eurocopter Experience in Flight Loop Development for Level D Training Simulator,” 30th European Rotorcraft Forum, Marseille, France, September 14-16, 2004.

²⁵Gubbels, A.W., Dillon, J., and Alexander, M., “Development of a Rotor State Measurement System for the NRC Bell 412 Advanced Systems Research Aircraft,” 59th Annual Forum of the American Helicopter Society, Phoenix, Arizona, May 6-8, 2003.

²⁶Manimala, B., Walker, D.J., Padfield, G.D., Voskuijl, M., and Gubbels, A.W., “Rotorcraft Simulation Modelling and Validation for Control Law Design,” *The*

Aeronautical Journal, Vol. 111, (1116), 2007, pp. 77-88, DOI: 10.1017/S0001924000001780.

²⁷Padfield, G.D., and White, M.D., “Measuring Simulation Fidelity Through an Adaptive Pilot Model,” *Aerospace Science and Technology*, Vol. 9, (5), 2005, pp. 400-408, DOI: 10.1016/j.ast.2005.03.004.

²⁸White, M.D., Perfect, P., Padfield, G.D., Gubbels, A.W., and Berryman, A.C., “Acceptance Testing and Commissioning of a Flight Simulator for Rotorcraft Simulation Fidelity Research,” *Proceedings of the Institution of Mechanical Engineers, Part G: Journal of Aerospace Engineering*, Vol. 227, (4), 2013, pp. 663-686, DOI: 10.1177/0954410012439816.

²⁹Perfect, P., White, M.D., Padfield, G.D., and Gubbels, A.W., “Rotorcraft Simulation Fidelity: New Methods for Quantification and Assessment,” *The Aeronautical Journal*, Vol. 117, (1189), 2013, pp. 235-282, DOI: 10.1017/S0001924000007983.

³⁰Anon., “FAA 14 Part 60 Flight Simulation Training Device Initial and Continuing Qualification and Use, Appendix C to Part 60-Qualification Performance Standards for Helicopter Full Flight Simulators,” 2016.

³¹Roesch, P., “Aerodynamic Design of the Aerospatiale SA 365N Dauphin 2 Helicopter,” *Journal of the American Helicopter Society*, Vol. 27, (2), 1982, pp. 27-33, DOI: 10.4050/JAHS.27.27.

³²Huber, H., and Masue, T., “Flight Characteristics Design and Development of the MBB/KHI BK 117 Helicopter,” 7th European Rotorcraft and Powered Lift Aircraft Forum, Garmisch Partenkirchen, Germany, September 8-11, 1981.

List of Figures

Fig. 1. Comparison of SID estimates from flight, and simulation predictions of the LDO mode characteristics with handling qualities boundaries (from Padfield (Ref. 1)).	27
Fig. 2. Yaw and roll response of Puma to pedal doublet input in (left) descending, (middle) level and (right) climbing flight at 80kts (Ref. 1).	27
Fig. 3. Unstable Dutch roll for the Super Puma at 125kts (Ref. 23).	27
Fig. 4. NRC Bell 412 ASRA.	28
Fig. 5. F-B412 LDO root loci for varying forward speed (10 kts intervals).	28
Fig. 6. Effect of flight path angle on the F-B412 LDO roll/yaw ratio at 90 kts.	29
Fig. 7. Effect of flight path angle on the stability of F-B412 LDO at 90kts.	29
Fig. 8. Comparison of responses to lateral cyclic (left) and pedal (right) inputs at 90kts.	30
Fig. 9. Comparison of responses of SID models with FT and the F-B412 to lateral cyclic (left) and pedal (right) inputs at 90kts.	31
Fig. 10. Comparison of LDO characteristics; SID estimates from flight and predictions from the linearized F-B412.	32
Fig. 11. Renovation flow chart.	32
Fig. 12. Comparison of responses of FT with F-B412 before and after renovation; lateral cyclic (left) pedal (right) inputs at 90kts.	33
Fig. 13. LDO characteristics of F-B412 before and after renovation compared with flight.	33
Fig. 14. Contributions of various F-B412 components to the weathercock stability from hover to 90kts (10kt increments from left to right).	34
Fig. 15. Impact of main rotor wake interference on the response to the pedal multi-step input.	34

Fig. 16. Impact of dynamic pressure loss at the tail on N_v (left) and LDO eigenvalue (right).35

Fig. 17. Impact of dynamic pressure loss at tail on the response to the pedal multi-step input.35

Fig. 18. Contribution of N_v to the yaw response from pedal input.....36

List of Tables

Table 1. F-B412 model parameters.....	37
Table 2. Variation of F-B412 derivatives Lv and Nv with flight path angle at 90 knots (climb, level and descent)	38
Table 3. Stability and control derivatives from the 3DoF LF-B412 and SID (FT) (90kts)	38
Table 4. LDO eigenvalues from FT, 3DoF and 6DoF models	39
Table 5. Renovation of the F-B412 for LDO.....	40
Table 6. LDO mode eigenvalues for the RF-B412 model	40

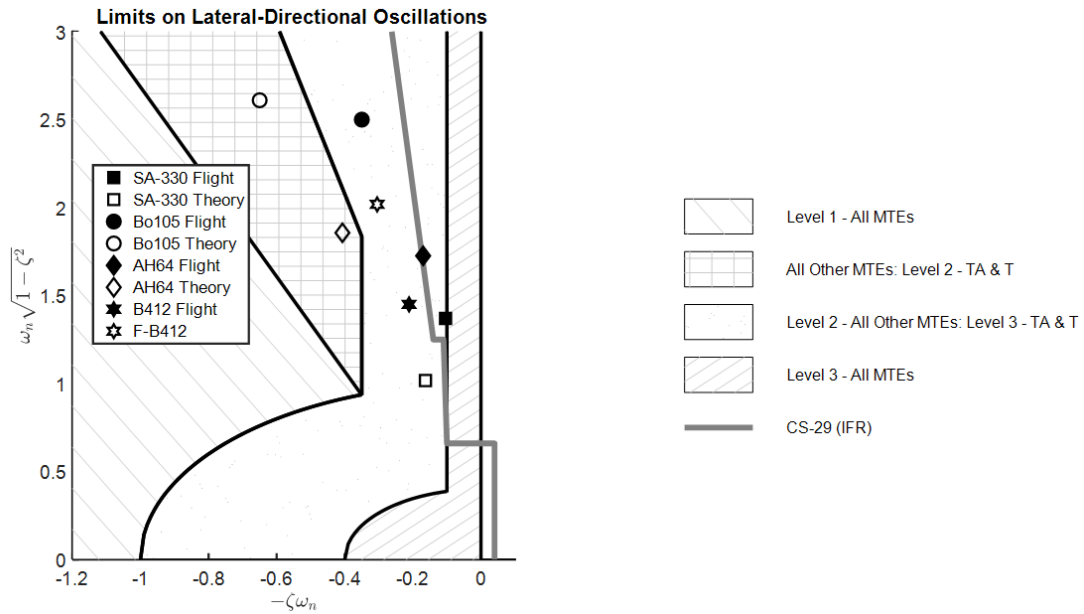


Fig. 1. Comparison of SID estimates from flight, and simulation predictions of the LDO mode characteristics with handling qualities boundaries (from Padfield (Ref. 1)).

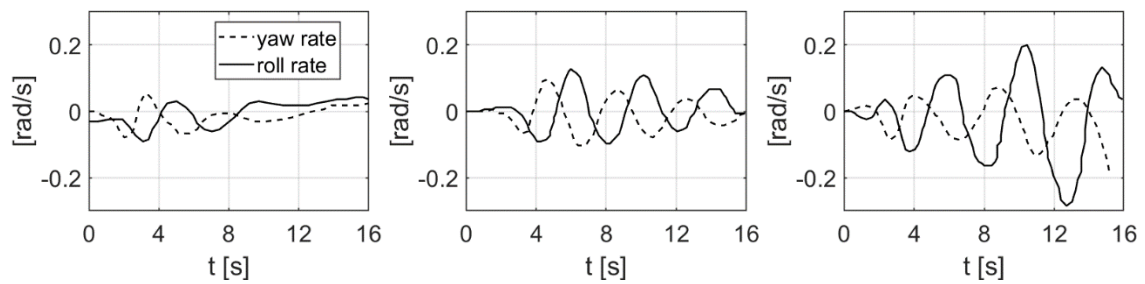


Fig. 2. Yaw and roll response of Puma to pedal doublet input in (left) descending, (middle) level and (right) climbing flight at 80kts (Ref. 1).

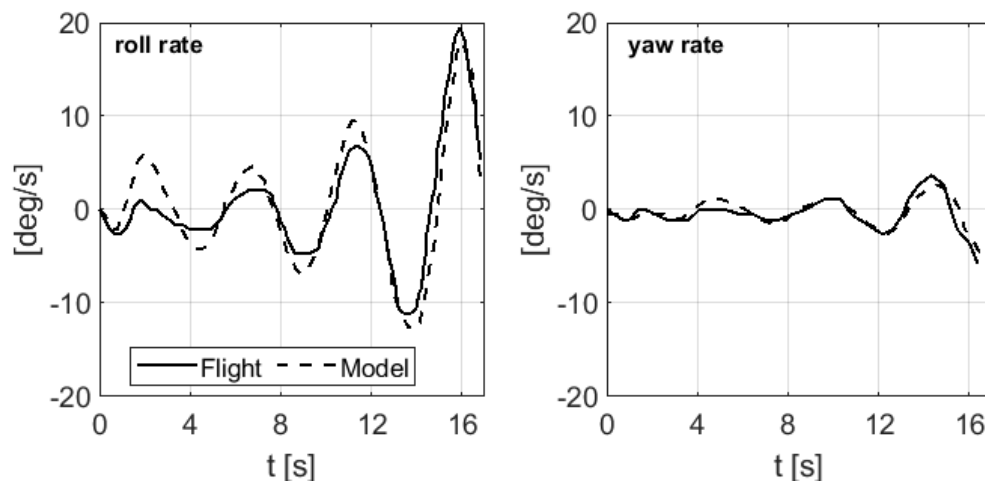


Fig. 3. Unstable Dutch roll for the Super Puma at 125kts (Ref. 24).



Fig. 4. NRC Bell 412 ASRA.

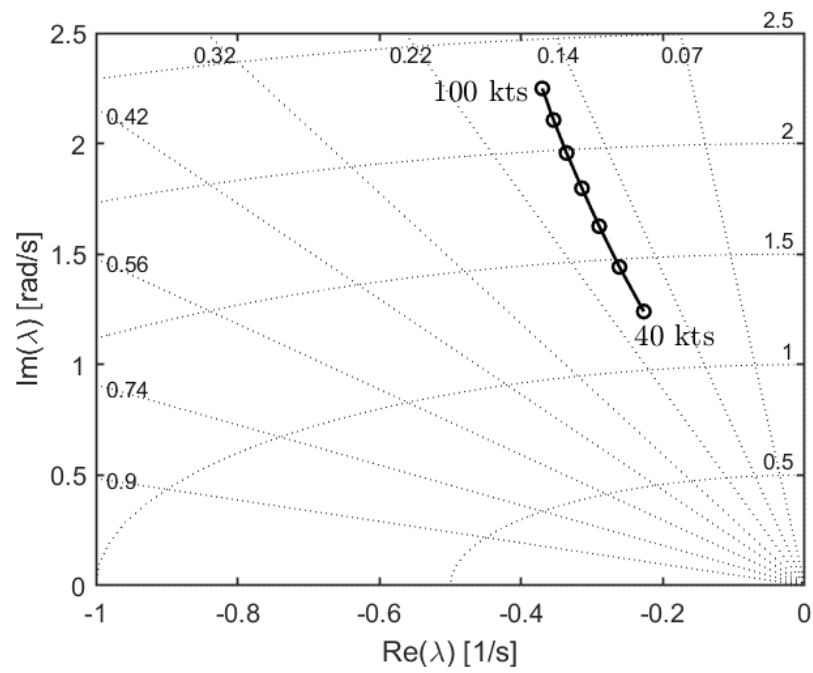


Fig. 5. F-B412 LDO root loci for varying forward speed (10 kts intervals).

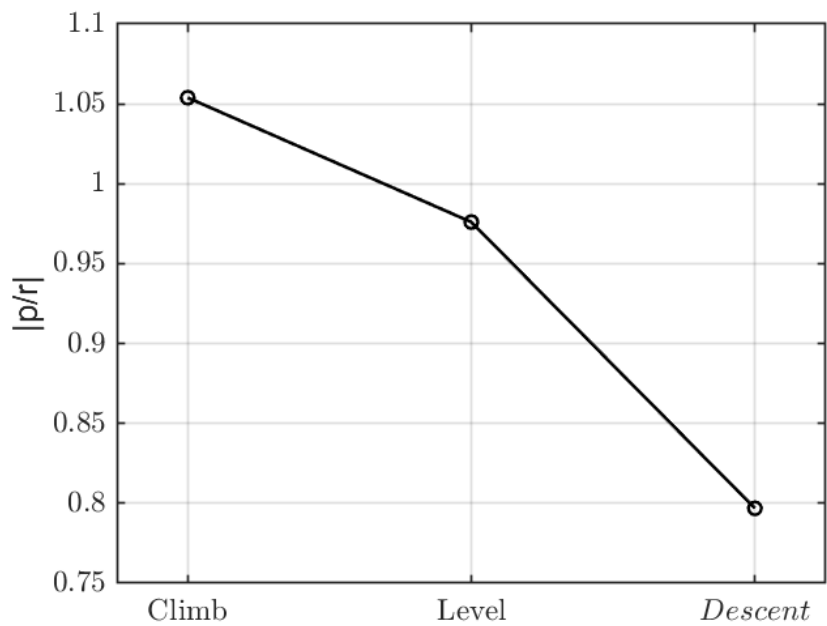


Fig. 6. Effect of flight path angle on the F-B412 LDO roll/yaw ratio at 90 kts.

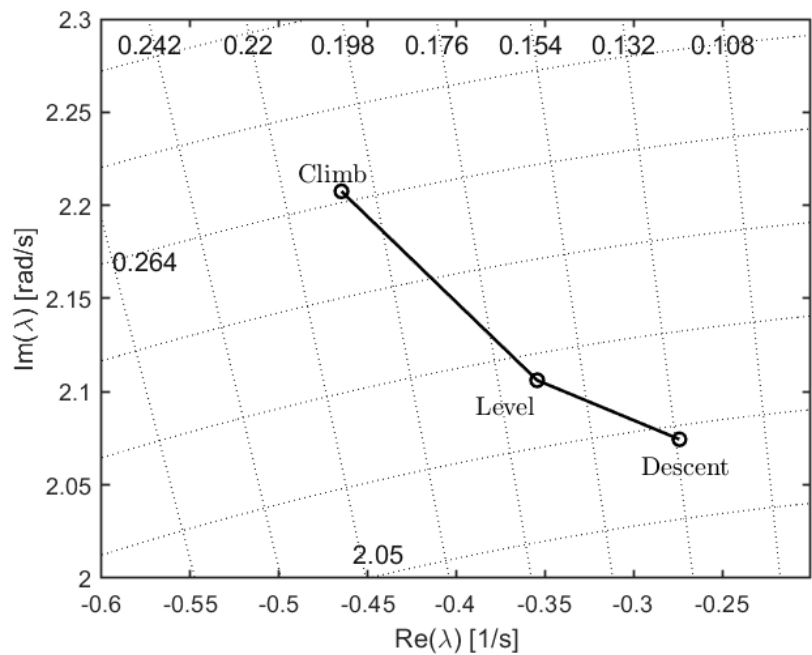


Fig. 7. Effect of flight path angle on the stability of F-B412 LDO at 90kts.

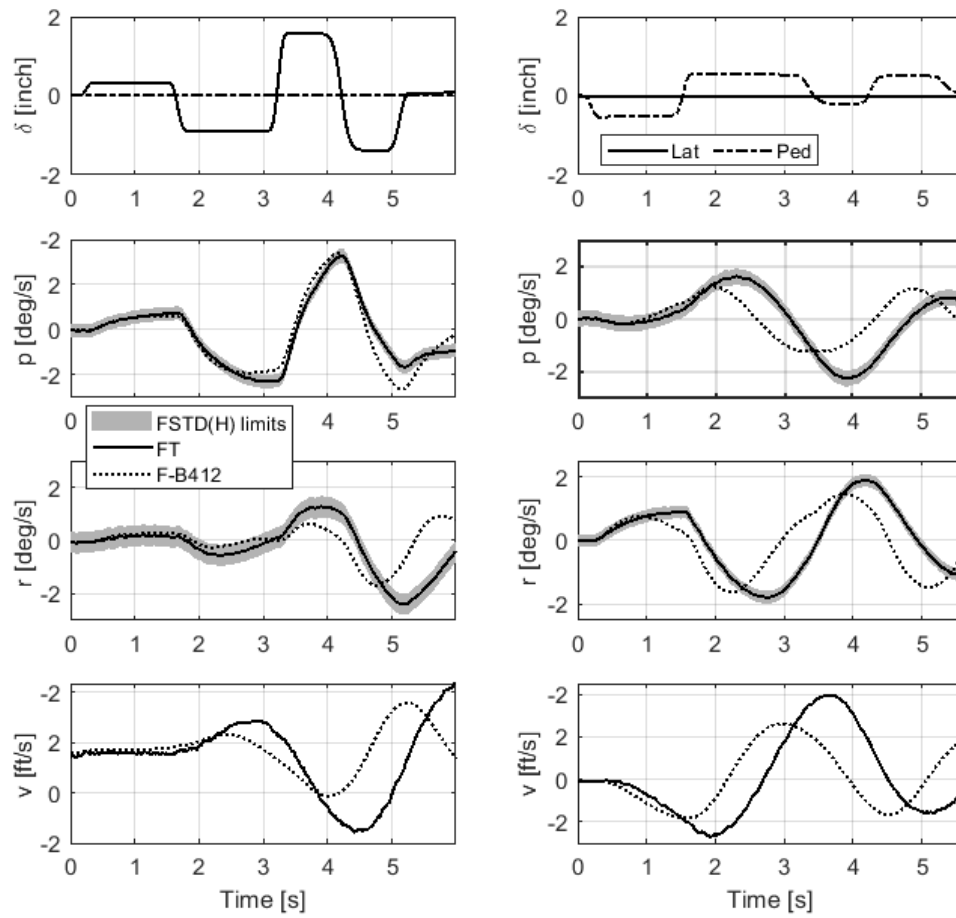


Fig. 8. Comparison of responses to lateral cyclic (left) and pedal (right) inputs at 90kts.

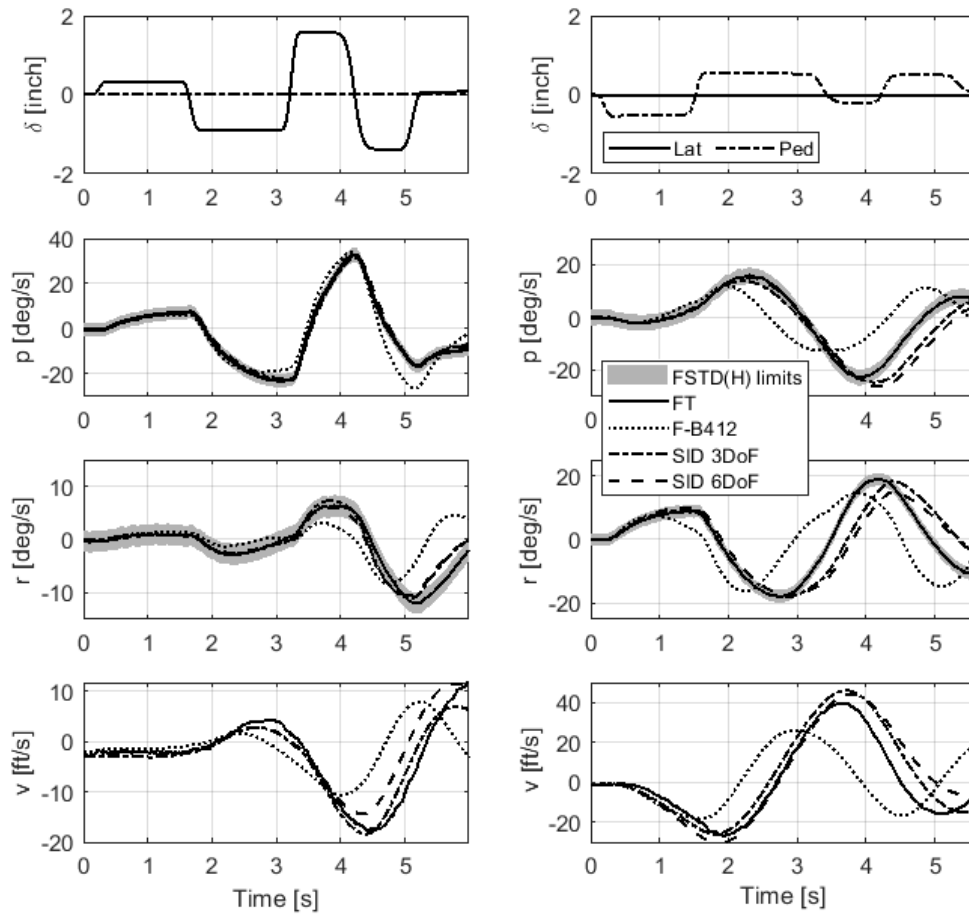


Fig. 9. Comparison of responses of SID models with FT and the F-B412 to lateral cyclic (left) and pedal (right) inputs at 90kts.

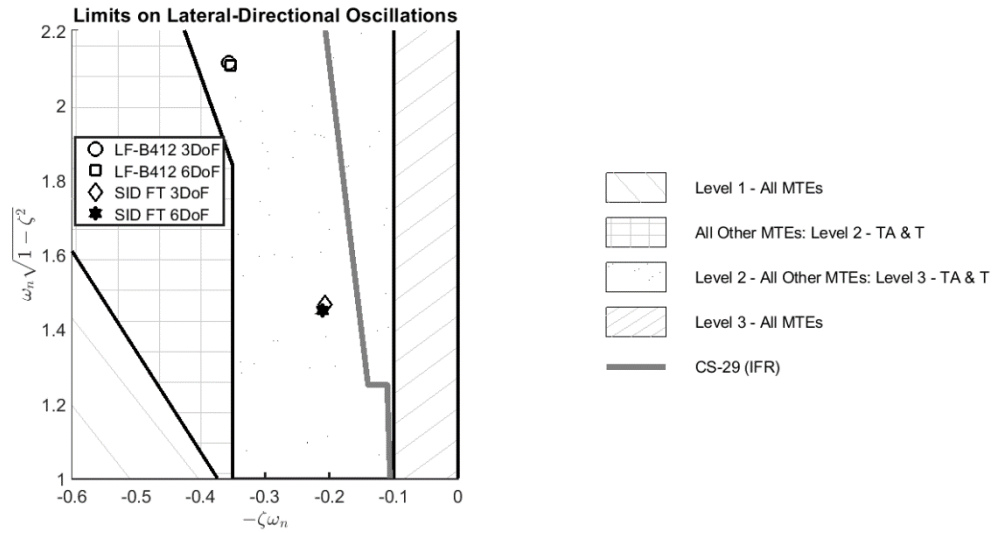


Fig. 10. Comparison of LDO characteristics; SID estimates from flight and predictions from the linearized F-B412.

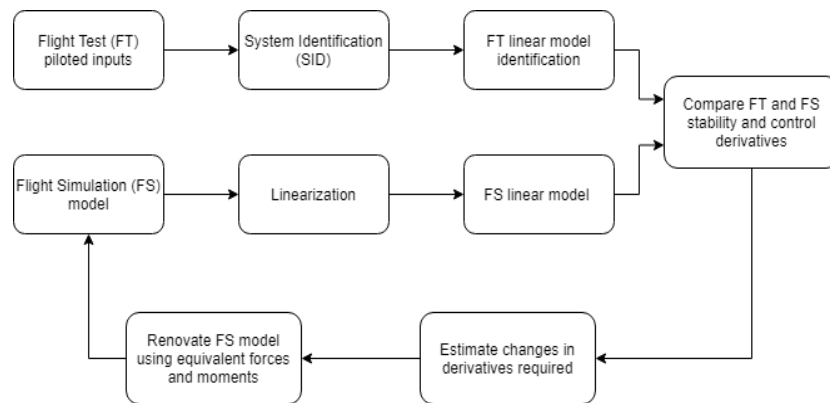


Fig. 11. Renovation flow chart.

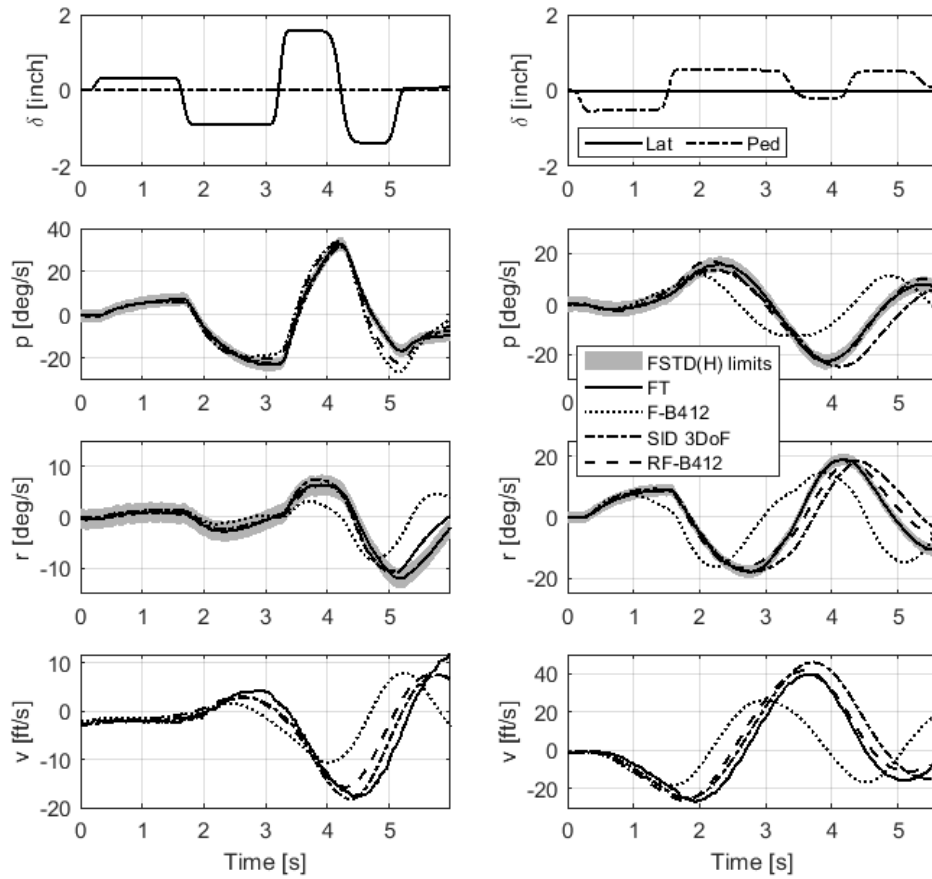


Fig. 12. Comparison of responses of FT with F-B412 before and after renovation; lateral cyclic (left) pedal (right) inputs at 90kts.

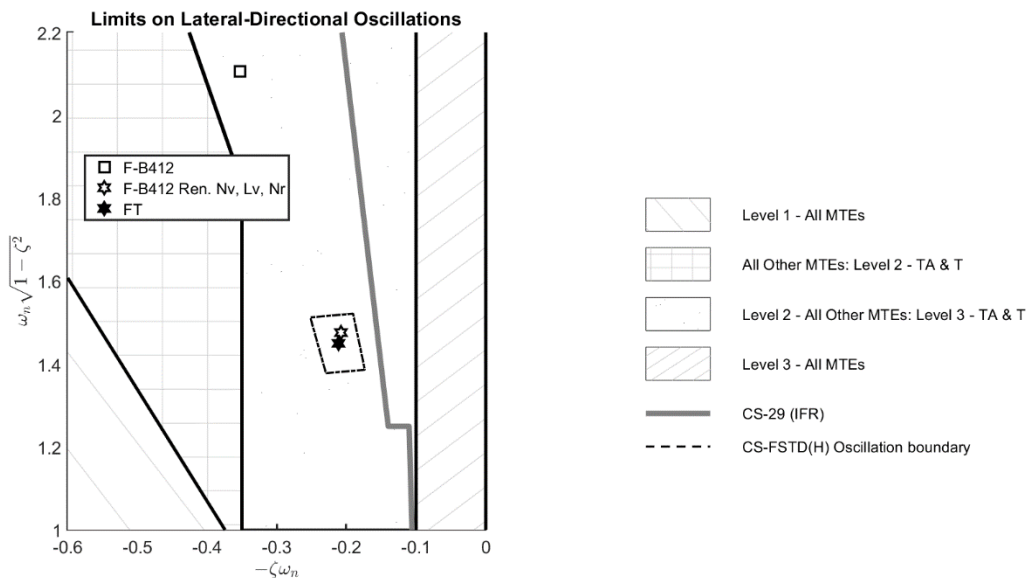


Fig. 13. LDO characteristics of F-B412 before and after renovation compared with flight.

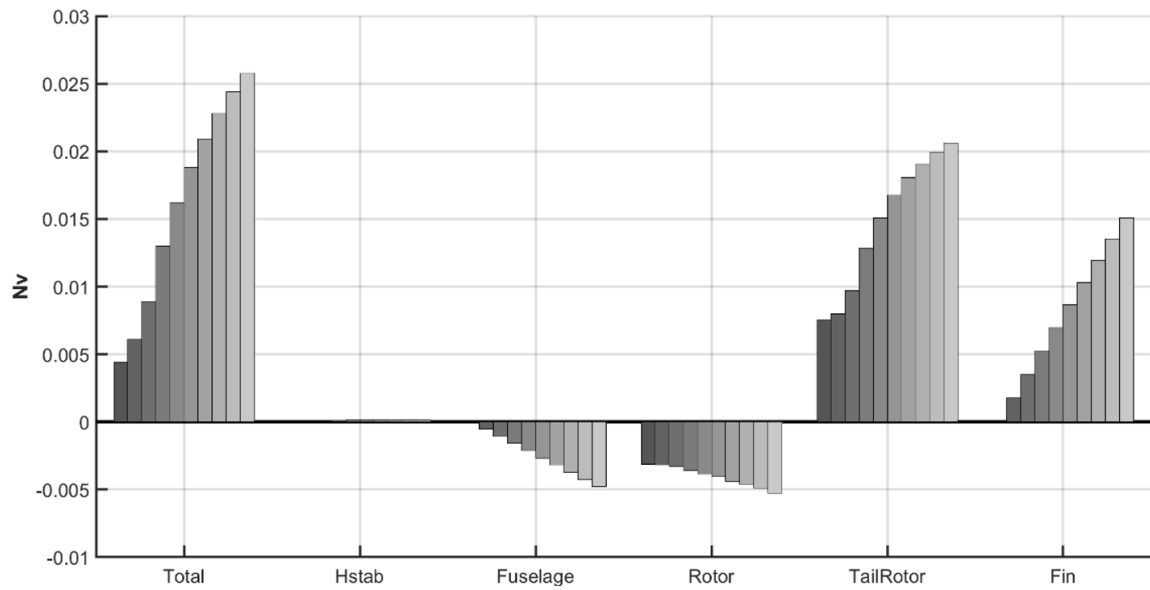


Fig. 14. Contributions of various F-B412 components to the weathercock stability from hover to 90kts (10kt increments from left to right).

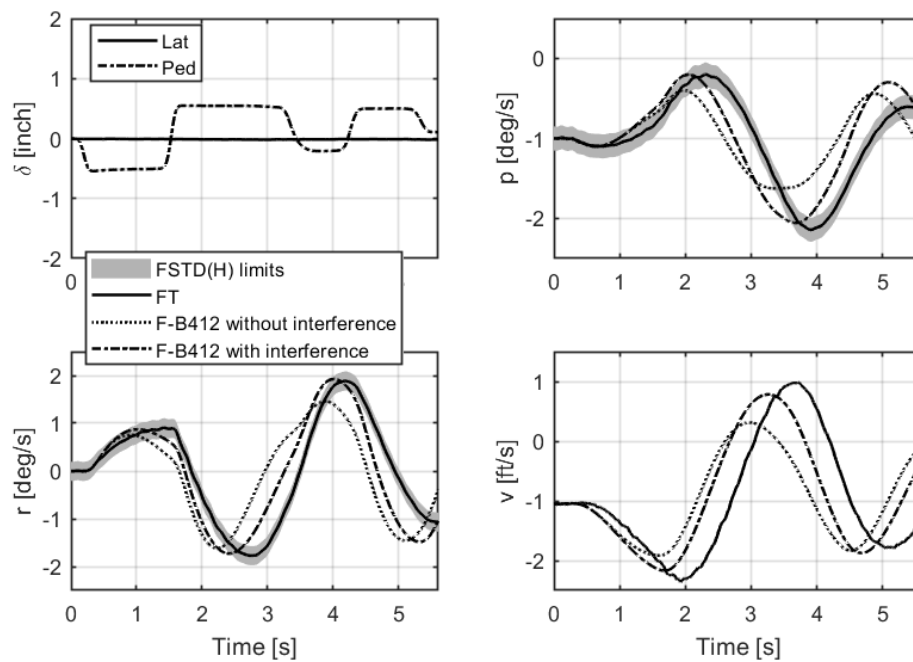


Fig. 15. Impact of main rotor wake interference on the response to the pedal multi-step input.

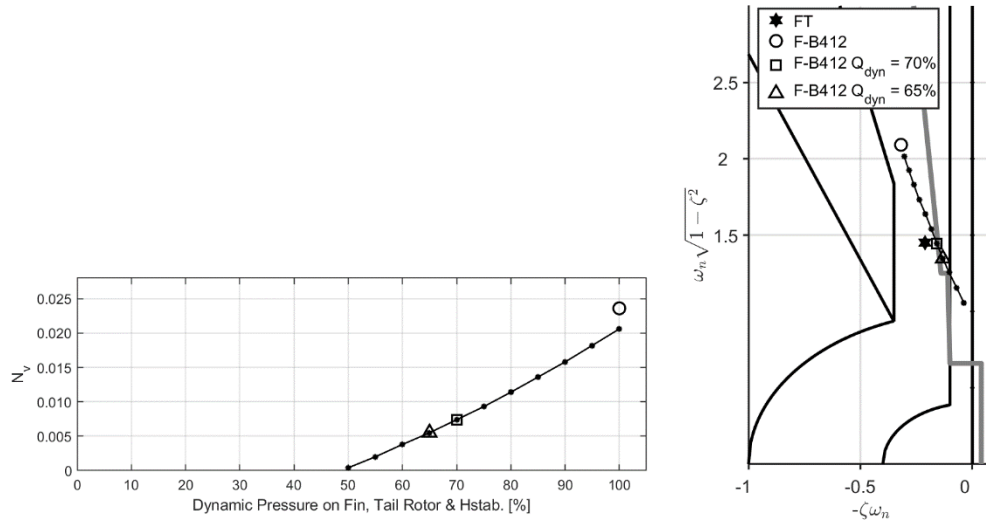


Fig. 16. Impact of dynamic pressure loss at the tail on N_v (left) and LDO eigenvalue (right).

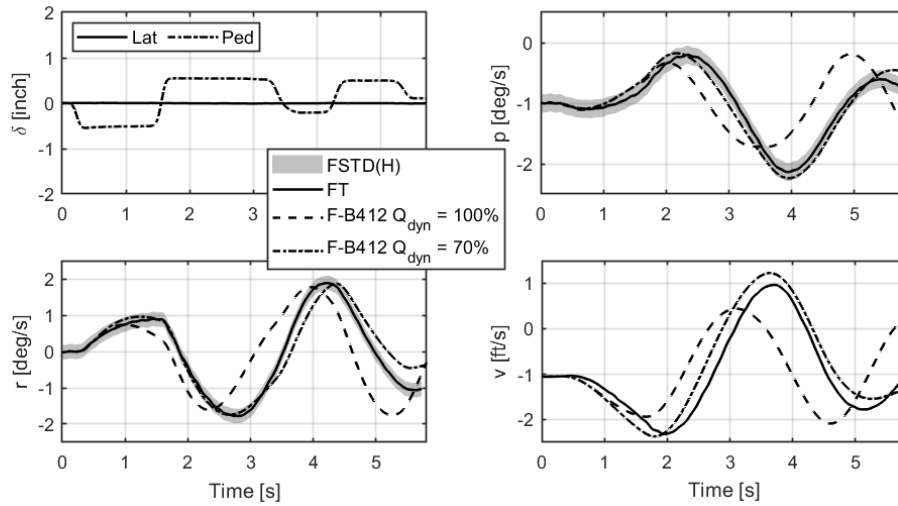


Fig. 17. Impact of dynamic pressure loss at tail on the response to the pedal multi-step input.

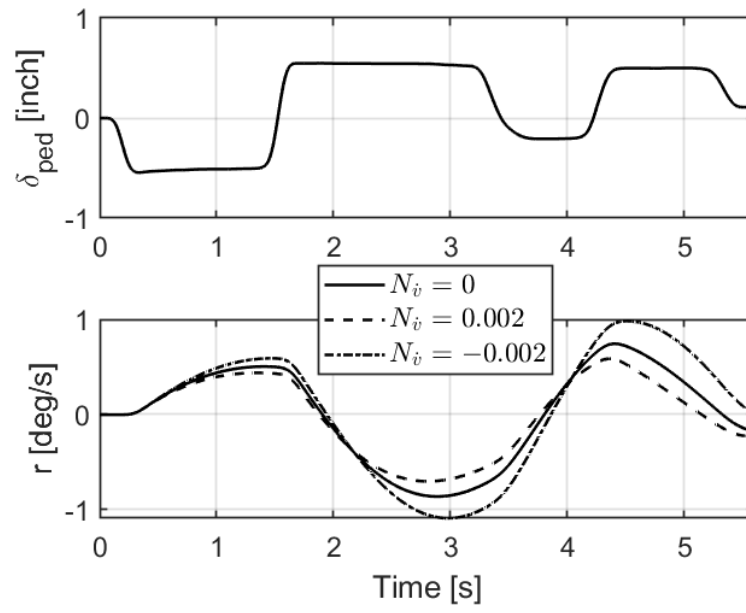


Fig. 18. Contribution of N_v to the yaw response from pedal input.

Table 1. F-B412 model parameters

Parameter	Value	unit
Inertias (Fuselage + Rotors)		
Mass	10290	lb
I_{xx}	4500	slug-ft ²
I_{yy}	16524	slug-ft ²
I_{zz}	14630	slug-ft ²
I_{xz}	2187	slug-ft ²
Main Rotor		
Rotor Speed (Ω)	33.9	rad/s
Swashplate Phase Angle	13	deg
Flap spring stiffness K_β	16700	ft-lbf/rad
Lag spring stiffness K_ζ	380840	ft-lbf/rad
Polar moment of inertia	2820	slug-ft ²
Blade		
Radius	23	ft
Chord	1.3	ft
Twist	-10.3	deg
Inboard aerofoil section	vr7	---
Outboard aerofoil section	OA309	---

Blade first moments of inertia M_β, M_ζ	59	slug-ft
Blade 2 nd moments of inertia I_β, I_ζ	790	slug-ft ²
Tail Rotor		
No. of blades	2	---
Radius	4.3	ft
Chord	0.96	ft
Aerofoil section	NACA0012	---
Tail rotor speed (Ω_{TR})	174	rad/s
Blade 2 nd moment of inertia $I_{\beta(TR)}$ per blade	1.45	slug-ft ²

Table 2. Variation of F-B412 derivatives L_v and N_v with flight path angle at 90 knots (climb, level and descent)

	L_v	N_v
Climb	-0.0381	0.0239
Level	-0.0367	0.0236
Descent	-0.0331	0.0261

Table 3. Stability and control derivatives from the 3DoF LF-B412 and SID (FT) (90kts)

Derivatives	FT	std	LF-	Derivatives	FT	std	LF-
			B412				B412

Y_v	-0.1309	0.0115	-0.1107	Y_{lat}	3.0050	0.1447	0.7687
Y_p	3.3380	0.5443	4.8673	Y_{ped}	0.0 [‡]	--	1.1867
Y_r	-164.6	1.0760	-158.51	L_{lat}	0.8639	0.0399	0.9269
L_v	-0.0248	0.0021	-0.0367	L_{ped}	0.2832	0.0192	0.3662
L_p	-2.1250	0.1125	-2.5160	N_{lat}	0.2233	0.0094	0.1674
L_r	0.0 [‡]	--	0.0340	N_{ped}	-0.5528	0.0231	-0.6706
N_v	0.0072	0.0006	0.0236	τ_{lat}	0.0800	0.0067	n/a
N_p	-0.5631	0.0378	-0.4523	τ_{ped}	0.1056	0.0062	n/a
N_r	-0.8066	0.0646	-1.0293				

[‡]Deleted in the model structure

Table 4. LDO eigenvalues from FT, 3DoF and 6DoF models

Derivatives	Eigenvalues (Exact)			Approx. Eigenvalues (Ref. 1)		
		ω_n	ζ		ω_n	ζ
LF-B412 3DoF	$-0.356 \pm 2.112i$	2.14	0.17	$-0.268 \pm 2.342i$	2.36	0.11
FT 3DoF	$-0.207 \pm 1.466i$	1.48	0.14	$-0.129 \pm 1.622i$	1.63	0.08
LF-B412 6DoF	$-0.354 \pm 2.107i$	2.14	0.17	$-0.268 \pm 2.342i$	2.36	0.11
FT 6DoF	$-0.211 \pm 1.450i$	1.47	0.14	$-0.145 \pm 1.476i$	1.48	0.10

Table 5. Renovation of the F-B412 for LDO

Derivative	Δ value change	% Δ change
L_v	0.0120	-32.5%
N_v	-0.0164	-69.5%
N_r	0.2227	-21.6%
N_{ped}	0.1178	-17.5%

Table 6. LDO mode eigenvalues for the RF-B412 model

Derivatives	Eigenvalues (Exact)	Approx. Eigenvalues (Ref. 1)				
		ω_n	ζ		ω_n	ζ
F-B412	$-0.3540 \pm 2.107i$	2.14	0.165	$-0.2677 \pm 2.342i$	2.36	0.113
F-B412 ren. N_v	$-0.1176 \pm 1.487i$	1.49	0.079	$-0.1353 \pm 1.730i$	1.73	0.078
F-B412 ren. L_v	$-0.4804 \pm 2.114i$	2.17	0.221	$-0.4484 \pm 2.297i$	2.34	0.192
F-B412 ren. N_r	$-0.2601 \pm 2.145i$	2.16	0.120	$-0.1675 \pm 2.359i$	2.36	0.071
F-B412 ren. $N_v L_v$	$-0.2828 \pm 1.429i$	1.45	0.195	$-0.3182 \pm 1.654i$	1.68	0.189
F-B412 ren. $N_v L_v N_r$	$-0.2078 \pm 1.476i$	1.49	0.141	$-0.2214 \pm 1.655i$	1.67	0.132
FT 3DoF	$-0.2071 \pm 1.466i$	1.48	0.141	$-0.1291 \pm 1.622i$	1.63	0.079
FT 6DoF	$-0.2113 \pm 1.450i$	1.46	0.146	$-0.1450 \pm 1.476i$	1.48	0.098